# Versatile patterns in the actin cortex of motile cells: Self-organized pulses can coexist with macropinocytic ring-shaped waves

**Arik Yochelis**[1,2*], **Sven Flemming**[3], **Carsten Beta**[3*]

***For correspondence:**
yochelis@bgu.ac.il (AY);
beta@uni-potsdam.de (CB)

[1]Department of Solar Energy and Environmental Physics, Blaustein Institutes for Desert Research (BIDR), Ben-Gurion University of the Negev, Sede Boqer Campus, Midreshet Ben-Gurion, 8499000, Israel; [2]Department of Physics, Ben-Gurion University of the Negev, Be'er Sheva 8410501, Israel; [3]Institute of Physics and Astronomy, University of Potsdam, Potsdam, 14476, Germany

**Abstract** Self-organized cortical actin patterns are essential for eukaryotic cellular life. They are the building blocks of many functional structures that often operate simultaneously, such as phagocytic cups and pseudopodia. However, the formation mechanisms underlying these versatile spatiotemporal forms remain poorly understood. In this context, it is a central challenge to identify how qualitatively distinct actin patterns can coexist. Here, we use giant cells of the social amoeba *Dictyostelium discoideum* together with mathematical theory to study a first paradigmatic example of pattern coexistence in the actin system. We report the emergence of a new type of narrow, planar, and fast-moving excitable pulse that coexists with the well-known ring-shaped macropinocytic actin waves. The study presents a blueprint for addressing the coexisting dynamical structures in cells and provides a first step toward a mechanistic understanding of cortical functions as well as a prerequisite for synthetic reconstitutions of cellular cortices.

## Introduction

In biological cells, many functional processes take place simultaneously. Key examples are observed in the actin cortex of eukaryotic cells, which is a dense, dynamic biopolymer network located at the inner face of the plasma membrane. Here, important cellular functions, such as phagocytosis, motility, and division, rely on a well-controlled orchestration of cortical activities in space and time ***Doherty and McMahon*** (***2009***); ***Goehring and Grill*** (***2013***); ***Fededa and Gerlich*** (***2012***); ***Blanchoin et al.*** (***2014***); ***Masters et al.*** (***2016***); ***Michaud et al.*** (***2021***). They self-organize both at the level of the actin cytoskeleton and in the upstream biochemical and mechanical signaling pathways ***Gerisch et al.*** (***2004***); ***Shibata et al.*** (***2012***); ***Luo et al.*** (***2013***); ***Tee et al.*** (***2015***); ***Bement et al.*** (***2015***); ***Lomakin et al.*** (***2015***); ***Negrete Jr et al.*** (***2016***); ***Diz-Muñoz et al.*** (***2016***); ***Stankevicins et al.*** (***2020***); ***Liu et al.*** (***2021***). Consequently, self-organization of cortical actin into a rich variety of patterns occurs; these patterns often appear simultaneously and have been abundantly observed in many cell types, such as neurons, dendritic cells, and neutrophils ***Hoon et al.*** (***2012***); ***Allard and Mogilner*** (***2013***); ***Beta and Kruse*** (***2017***). Understanding how cells can generate and robustly maintain qualitatively different coexisting patterns has thus become one of the paramount challenges of modern life sciences. It

is fundamental not only to cellular life and to pathologies, such as cancer ***Orth and McNiven*** (***2006***); ***Hoon et al.*** (***2012***), but also can serve as a roadmap to the emerging field of synthetic biology, for which minimal candidate systems are required to robustly mimic intracellular spatiotemporal behaviors.

While recent research has primarily addressed the emergence of cortical actin waves that exhibit well defined wavelengths or temporal periods ***Allard and Mogilner*** (***2013***); ***Beta and Kruse*** (***2017***), the coexistence of different patterns has been largely ignored and remains poorly understood. Here we present unexpected experimental evidence from microscopy recordings of giant amoeboid cells, showing that different types of dynamical patterns can be simultaneously maintained in the actin cortex of living cells. Specifically, we reveal a distinct generic mechanism that relies on actin conservation, by which excitable and oscillatory waves emerge and coexist in the cell cortex. This observation offers a promising opportunity to study the subcellular coexistence of space-time patterns by focusing on the exemplary case of cortical actin waves. Our findings are intrinsically related to the complexity of biological systems, in which high-dimensional descriptions result in dynamical instabilities that cannot be observed in low-dimensional models with only two dynamical variables ***Holmes and Edelstein-Keshet*** (***2012***); ***Rappel and Edelstein-Keshet*** (***2017***) — an insight that dates back to Alan Turing's seminal work on morphogenesis ***Turing*** (***1952***).

## Results

### Experimental observation of waves and pulses

A well-established model organism to study the dynamics of the actin cortex is the social amoeba *Dictyostelium discoideum*. In *D. discoideum*, actin waves were reported more than 20 years ago ***Vicker et al.*** (***1997***), and they have been intensively studied with respect to their dynamics, structure, and biochemical composition ***Gerisch et al.*** (***2004***); ***Shibata et al.*** (***2012***); ***Asano et al.*** (***2008***); ***Jasnin et al.*** (***2019***). At the cytoskeletal level, these waves consist of traveling domains of increased F-actin concentration that are surrounded by a dense ring of F-actin. In terms of geometry and composition, they resemble endocytic structures and are, most likely, frustrated macropinocytic cups that cannot evolve into a full three-dimensional structure due to the rigid cover slip surface ***Gerisch et al.*** (***2009***). In particular, similar to macropinocytic cups, basal actin waves critically depend on Ras signaling. Their formation is stimulated by a deficiency in Ras-GAP NF1, which is typical for the commonly used axenic lab strains and which also increases the size of the macropinocytic cups ***Veltman et al.*** (***2016***). A particular advantage of the *D. discoideum* model system is the possibility to increase its cell size by electric-pulse-induced cell fusion, so that actin wave dynamics can be observed over large intact cell cortices independent of boundary effects ***Gerisch et al.*** (***2013***). In these giant cells, they take the form of actin-rich, band-shaped structures that travel at a characteristic speed and constantly split and coalesce in an irregular fashion ***Gerhardt et al.*** (***2014***); ***Miao et al.*** (***2019***); ***Flemming et al.*** (***2020***).

These well-known basal waves have been mostly described for axenic cell lines that feed on a liquid growth medium by macropinocytic liquid uptake. To explore new regimes of cytoskeletal dynamics, we changed the growth conditions and cultured the commonly used axenic *D. discoideum* lab strain AX2 together with bacteria. When feeding on bacteria, cells strongly enhance their pseudopod-driven motility in order to increase their chances of finding localized food sources ***Paschke et al.*** (***2018***). Under these conditions, we expected pseudopod formation to compete with the formation of macropinocytic cups for the common actin pool. Also in this case, we observed basal actin waves that displayed the characteristic ring-shaped structure and meandering dynamics; see Fig. 1**a** and Movie 1. However, upon an increase in cell size, the cortical wave patterns exhibited an additional new feature that has not been observed in giant cells produced from axenically grown cells in the absence of bacteria. Namely, in addition to the well-known broad ring-shaped wave segments, the giant cells that were produced from cells grown on bacteria displayed sharp planar traveling pulses. These pulses behaved like genuine excitable solitary waves and have

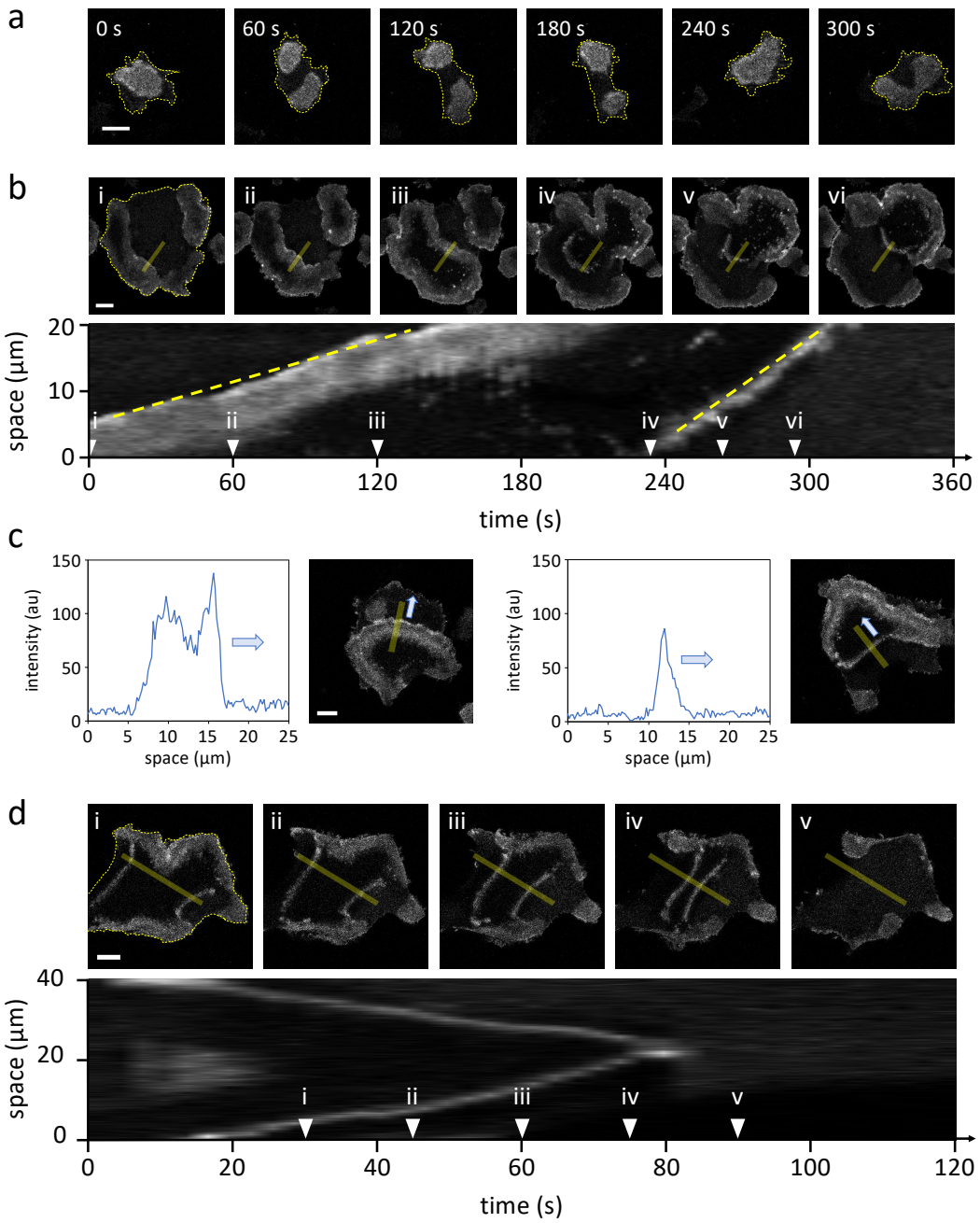


**Figure 1.** Coexisting waves and planar pulses in giant amoeboid cells. **(a)** Meandering and splitting actin wave in the ventral cortex of a *D. discoideum* cell. **(b)** Coexistence of slowly moving broad actin waves and rapidly propagating planar pulses in the cortex of a giant *D. discoideum* cell. The kymograph on the bottom row was taken along the yellow line displayed in the snapshots above. The dashed yellow lines are visual guides, indicating the different speeds of the wave and the pulse propagation. **(c)** Actin profiles of a wave (left) and a pulse (right) together with their respective snapshots; the yellow lines show the position where the profile was recorded, and the arrow indicates the direction of the wave and the pulse propagation, respectively. **(d)** Head-on collision and mutual annihilation of two counter-propagating planar pulses. The kymograph on the bottom row was taken along the yellow line displayed in the snapshots above. Dashed yellow lines in **a**, **b**, and **d** are visual guides that indicate the cell outline and all scale bars correspond to 10 $\mu$m.

hitherto not been observed.

Both types of wave patterns—the broad macropinocytic traveling waves and the sharp planar pulses—coexist in the same giant cell, and in Fig. 1**b**, we show that they are distinct from each other in their profiles and propagation speeds, see also Movie 2. The planar pulses propagate at a higher speed than the broad traveling waves, and their profile is sharply peaked as compared to the wider profile of the traveling waves, which exhibit characteristic actin peaks at their leading and trailing edges. The latter results from the ring-shaped structure of the frustrated cup (see Fig. 1**c**), a feature that is well known from earlier reports ***Gerhardt et al.*** (***2014***). The planar pulses typically emerge near the cell border and travel straight across the substrate-attached bottom membrane. Upon head-on collision, the planar pulses mutually annihilate as expected; see Fig. 1**d** and Movie 3 for an example.

The unexpected experimental observation of two markedly distinct coexisting wave patterns—periodically reappearing traveling waves and seldom emerging planar pulses—is supported by a generic theory that reveals the minimal conditions for such a coexistence, relying on an activator-inhibitor framework with conservation of mass; here the total concentration of actin monomers is largely conserved within the time scales of wave dynamics.

## Uncovering the generic nature of planar pulses via actin conservation

Intracellular actin dynamics involves multiple spatiotemporal feedbacks ranging from the molecular level of protein kinetics to mechanical membrane deformation ***Gerisch et al.*** (***2011***); ***Isaac et al.*** (***2013***); ***Allard and Mogilner*** (***2013***); ***Beta and Kruse*** (***2017***); ***Cao et al.*** (***2019***); ***Tamemoto and Noguchi*** (***2021***). Yet, it has already been shown that fundamental insights into actin wave dynamics can be obtained by approximate descriptions in terms of reaction-diffusion (RD) systems that reduce the complexity of the actin cortex to a small number of key components and incorporate their most salient interactions ***Bernitt et al.*** (***2017***). These include a conserved pool of actin that is either encountered in its monomeric form (G-actin) or may polymerize to filamentous cortical structures (F-actin). In addition, F-actin may autocatalytically enhance its own formation, which reflects the well-known branching mechanisms and positive feedback to the activatory components of the upstream signaling pathway, such as PI3K and Ras ***Sasaki et al.*** (***2007***). On the other hand, the growth of filamentous structures is counterbalanced by inhibitory regulators, such as Coronin or Aip1 ***Ishikawa-Ankerhold et al.*** (***2010***). This is typically taken into account by an effective inhibitory component that is triggered in the presence of F-actin and downregulates the rate of polymerization. An overall schematic representation of the components and their interactions is displayed in Fig. 2**a**.

In general, due to autocatalytic growth and nonlinear feedback, multiple stable states may emerge that are characterized by different F-actin concentrations. From the study of circular dorsal ruffles (CDRs), it is known that at least two stable uniform states can coexist (bistability) ***Bernitt et al.*** (***2017***): a state that shows only a small amount of filamentous actin and is consequently dominated by a high G-actin concentration ($\mathbf{P}_*^0$) and a state of high F-actin concentration ($\mathbf{P}_*^+$). For consistency, an unstable state at intermediate F-actin levels ($\mathbf{P}_*^-$) must also exist in this case, but it cannot be observed in experiments; see Fig. 2**b** for a schematic representation of the coexisting states.

As G-actin monomers are inherently present, $\mathbf{P}_*^0$ is assumed to be always stable, while the F-actin-rich state $\mathbf{P}_*^+$ may become unstable to give rise to spatiotemporal oscillations ***Allard and Mogilner*** (***2013***); ***Beta and Kruse*** (***2017***). Patterns that exhibit spatiotemporal dynamics typically emerge through generic instabilities. For a multi-component system as described in Fig. 2**c**, this occurs, most generally, via the oscillatory-wave codimension-2 bifurcation that requires the tuning of two parameters, here $A \to A_{\mathrm{HO}}$ and $D_{\mathrm{N}} \to D_{\mathrm{W}}$. In this case, it is coupled to a large-scale mode (LSM), also known as the Goldstone mode, due to mass conservation. Weakly nonlinear theory (center manifold reduction) demonstrates that the patterns forming near such a codimension-2

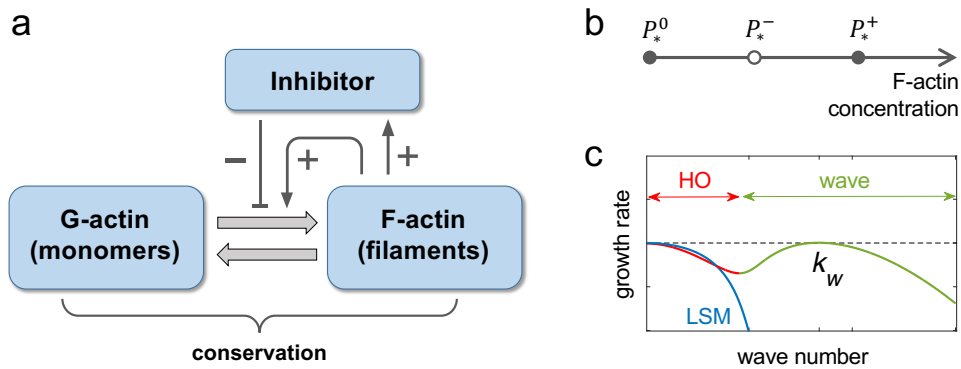


**Figure 2.** Schematic representation of the actin dynamics model and the arising instabilities. **(a)** Interaction network of the three components of the actin dynamics model. Mass conserved reactions are represented by thick light grey arrows. Activatory $(+)$, and inhibitory $(-)$ interactions are represented by thin dark grey arrows. **(b)** Stable (filled circles) and unstable (empty circle) fixed points as a function of F-actin concentration; depending on the parameters, $\mathbf{P}_*^+$ may become unstable. **(c)** Three growth rates associated with the real parts of the dispersion relations computed by the linearization of the mass conserved activator-inhibitor model (system (3) in Methods and Materials) about $\mathbf{P}_*^+$ at the codimension-2 point, $D_\mathrm{N} = D_\mathrm{W} \simeq 0.32$ and $A = A_\mathrm{HO} \simeq 11.7$ (other parameters as in Methods and Materials Eq. 4): simultaneous onset of homogeneous oscillations (HO, red) and traveling waves (wave, green) in the presence of a large-scale mode (LSM, blue) that is associated with mass conservation, displaying a persistent neutral mode (at zero wave-number).

point can be described by the following leading order approximation:

$$\mathbf{P}_*^+ \sim \{\underbrace{B_0(X,T)e^{i\omega_0 t}}_{\text{HO}} + \underbrace{B_L(X,T)e^{i\omega_W t + ik_W x} + B_R(X,T)e^{i\omega_W t - ik_W x}}_{\text{waves}} + c.c.\} + \underbrace{C(X,T)}_{\text{LSM}} + h.o.t., \tag{1}$$

where, $X, T$ are slow space and time scales as compared to $x, t$, respectively, so that complex amplitudes $B_0, B_{L/R}$ describe the weak spatiotemporal modulations of homogeneous oscillations (HO) associated with frequency $\omega = \omega_0$ and wavenumber $k = 0$, and the left/right propagating waves associated with $\omega = \omega_W$ and $k = k_W$ at the instability onset, respectively. The real valued field $C$ is associated with mass conservation, $c.c.$ stands for complex conjugated, and $h.o.t.$ stands for high order terms. This is further illustrated in Fig. 2**c**, where a schematic dispersion relation about the $\mathbf{P}_*^+$ state at the codimension-2 instability onset is shown. Here, the red branch represents the onset of homogeneous oscillations at $k = 0$, the green branch corresponds to the traveling wave instability at $k = k_W$, and the large-scale mode is represented in blue. We note that partial representations along the lines of (1) have been introduced without mass conservation in ***Falcke et al.*** (***1995***), while waves coupled to a conserved quantity (LSM) were initially introduced in ***Winterbottom et al.*** (***2005***). The approximation (1), however, is more general, exhibiting a seven-dimensional center manifold. Using standard symmetry considerations, the corresponding amplitude equations for $B_0$, $B_L$, $B_R$, and $C$ can also be specified in the weakly nonlinear regime; see Methods and Materials.

However, to explicitly address the coexistence of traveling waves (TWs) and excitable pulses (EPs), we have to rely on a specific model (see Methods and Materials), as EPs are highly nonlinear solutions. Consequently, we consider, without loss of generality, a reduced actin dynamics model that can be seen as a specific realization of the reaction scheme presented in Fig. 2**a** and has been numerically shown to exhibit EP and soliton-like dynamics ***Yochelis et al.*** (***2020***). We denote the F-actin concentration as $N(x,t)$, G-actin as $S(x,t)$, and the inhibitor as $I(x,t)$, so that the model phase space is spanned by $\mathbf{P} = (N, S, I)$, and the three uniform solutions are $\mathbf{P}_*^0 = (N_*^0, S_*^0, I_*^0)$, $\mathbf{P}_*^\pm = (N_*^\pm, S_*^\pm, I_*^\pm)$ (see Methods and Materials Eq. 5). In general, actin conservation implies that $L^{-1}\int_L \{N + S\}\mathrm{d}x = A$, where $A$ is the total actin concentration, and $L$ is the domain length. In what follows, both will be used as control parameters. The G-actin-dominated state $\mathbf{P}_*^0$ always exists and, within the range of parameters considered here, is also linearly stable. The two states $\mathbf{P}_*^\pm$ coexist

for $A > A_{\mathrm{SN}}$ ***Yochelis et al.*** (***2020***), where $\mathbf{P}_*^-$ is linearly unstable, and $\mathbf{P}_*^+$ is linearly stable for $A > A_{\mathrm{W}}$; see the bifurcation diagram in Fig. 3**b**. The condition $A > A_{\mathrm{W}}$ thus designates a bistable regime, where front solutions connecting $\mathbf{P}_*^0$ and $\mathbf{P}_*^+$ may form ***Bernitt et al.*** (***2017***).

We now concentrate on the instabilities of the $\mathbf{P}_*^+$ state that occur as $A$ is decreased. Without any loss of generality, we focus on a nonlinear parameter range that is far from the codimension-2 point (and only mention that the results also persist near the codimension-2 point). The analysis is performed using the spatial dynamics methodology that combines bifurcation theory and numerical continuation ***Doedel et al.*** (***2012***); see Methods and Materials for details. As $A$ is decreased, the uniform stable steady state $\mathbf{P}_*^+$ undergoes a wave (a.k.a. finite wavenumber Hopf) instability at $A_{\mathrm{W}}$, giving rise to traveling waves with wavenumber $k = k_W$; see also the dispersion relation in the left panel of Fig. 3**a**. In the bifurcation diagram in Fig. 3**b**, the primary $\mathrm{TW}_{\lambda_c}$ branch that emerges from $A_{\mathrm{W}}$ is displayed as a function of $A$ (green line). Each point along the $\mathrm{TW}_{\lambda_c}$ branch is associated with a periodic solution (with wavelength $\lambda_c = 2\pi/k_W$) and plotted as the maximal value of the $N$ component. The TW solutions bifurcate (super-critically) toward the unstable direction of $\mathbf{P}_*^+$ and are initially stable. Similarly, standing waves (SWs) also bifurcate from $A_{\mathrm{W}}$, but we only mention their coexistence without explicitly showing their branch. Upon an increase of the domain size to fill multiple copies of $\mathrm{TW}_{\lambda_c}$, a secondary instability of the Eckhaus-Benjamin-Feir type ***Janiaud et al.*** (***1992***) destabilizes the $\mathrm{TW}_{\lambda_c}$ solutions, and the instability onset saturates at $A \simeq 10.3$ for $L \sim O(10\lambda_c)$ (similarly as reported by ***Yochelis et al.*** (***2008***)); the instability point is marked in Fig. 3**c**, by the transition from a solid to a dashed line. As $A$ is decreased below $A_{\mathrm{W}}$, additional TWs with larger spatial periods than $\lambda_c$ emerge from the uniform state $\mathbf{P}_*^+$, and their stability is also extended to lower $A$ values; see Methods and Materials Fig. 5. We note that this behavior is generic and stems from the codimension-2 point (not shown here to avoid redundancy).

An increase in the domain size is also related to the emergence of homogeneous oscillations (HO) at $A = A_{\mathrm{HO}}$ (in addition to $\mathrm{TW}_{\lambda_c}$) for which the wave-number vanishes and the wavelength diverges; see the dispersion relation in the middle panel of Fig. 3**a**. Numerically, it is impossible to implement infinite domains, but the typical approximation of periodic boundary conditions holds for such purposes. The continuation of periodic solutions from $A_{\mathrm{HO}}$, in a large domain $L = 1000 \gg \lambda_c$ (red line in Fig. 3**b**), shows that far from the onset, these solutions eventually develop into EPs. This evolution is depicted in Fig. 3**c**, together with the respective profiles (Fig. 3**e**), along the branch in **c**. Up to the first sharp fold (homoclinic bifurcation in space) on the right (indicated by a triangle), the solutions are indeed periodic (with the period being as large as the domain size), and thus, at large amplitudes, they correspond to a broad pulse-like state; see Fig. 3**c** and the rightmost profile in **e**. The branch then proceeds to the left and up to another fold (indicated by a rectangle), where the profile approaches a genuine pulse solution (see panel **e**), yet this solution is unstable since it is embedded in the background of the unstable $\mathbf{P}_*^-$ state as $x \to \pm\infty$. Finally, after another fold at $A_{\mathrm{TP}}$ (indicated by a diamond), the branch extends to the left (toward $A_{\mathrm{TP}}^{\mathrm{SN}}$), and within this range, stable EPs emerge (as shown, for example, at the location indicated by a dot). Notably, the latter is embedded in the background of $\mathbf{P}_*^0$, as shown by the respective leftmost profile in **e**.

The transition from unstable to stable EP solutions corresponds to a generic global bifurcation that is also of codimension-2 and on an infinite line, also known as the T-point ***Glendinning and Sparrow*** (***1986***). This bifurcation designates the merging of two EPs (homoclinic orbits in space), creating a bounded front state (heteroclinic cycle in space) connecting bidirectionally (bi-asymptotically) two uniform solutions $\mathbf{P}_*^\pm$ as $x \to \pm\infty$ ***Romeo and Jones*** (***2003***). In Fig. 3**f**, we also schematically show the respective geometrical interpretation based on the profiles in **e**. It is then easy to see that while in large domains, the stability onset of EP is close to $A_{\mathrm{TP}}$, in small domains, where the excitation width of EP is on the order of the domain size, the onset shifts to lower $A$ values, as shown in Fig. 3**d**. This shift is associated with a structural change as the solutions depart from their solitary nature in space, becoming limit cycles (in space) rather than homoclinic orbits ***Glendinning and Sparrow*** (***1986***); see also Figs. 3**e**,**f**.

In an infinite domain, the stability of EPs persists from $A = A_{\mathrm{TP}} \approx A_{\mathrm{HO}}$ down to $A = A_{\mathrm{TP}}^{\mathrm{SN}}$ (see

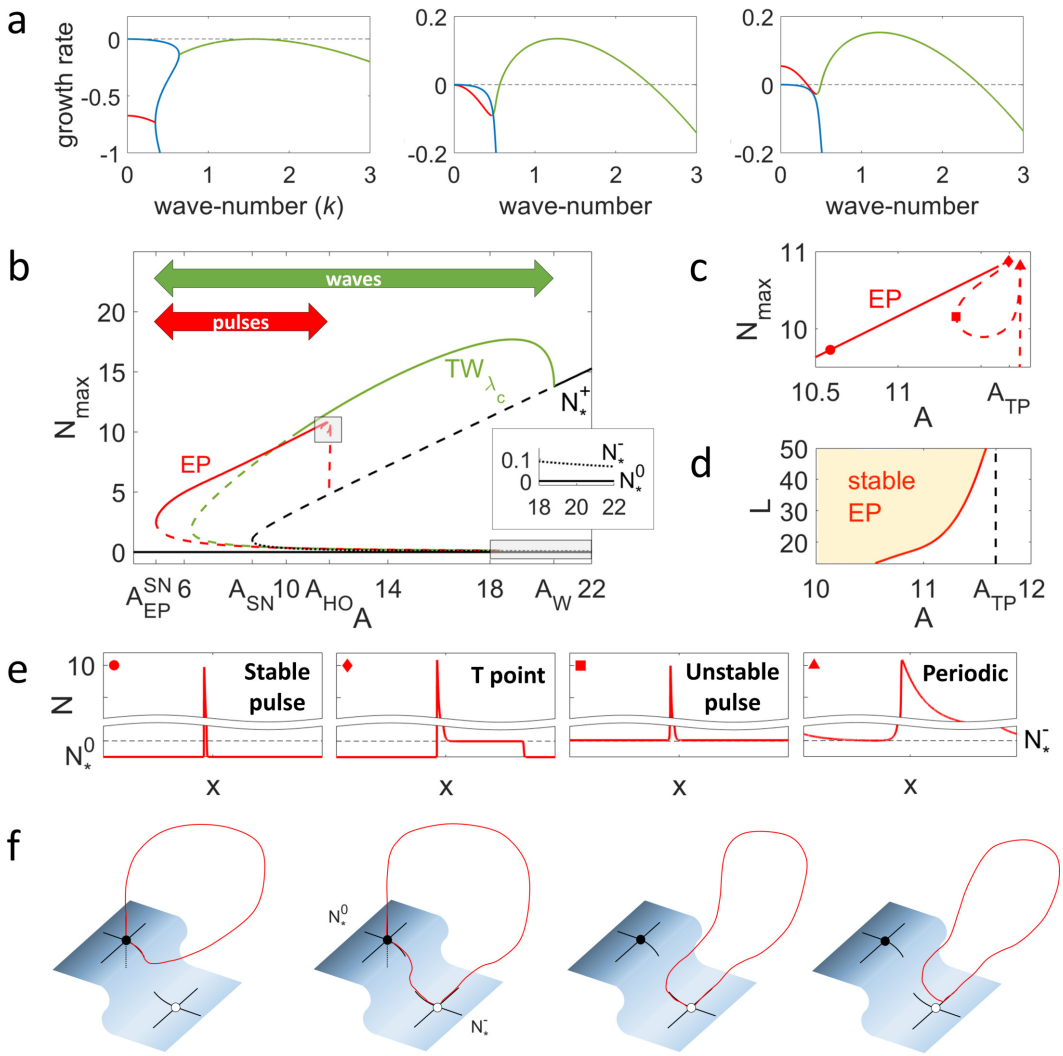


**Figure 3.** Analysis of the mass conserved activator-inhibitor model for waves and pulses (Methods and Materials Eqs. 3,4). **(a)** Growth rates as in Fig. 2**c**, at selected values of the total actin conservation, $A$. From left to right: the wave onset (green) at $A = A_{\mathrm{W}} \simeq 20.5$, the wave unstable regime with homogeneous oscillations (HO) neutral (red) at $A_{\mathrm{HO}} \simeq 11.7$, and an additional unstable regime at $A = 11$, where waves and HO are both unstable. The blue curve indicates real valued dispersion relations. **(b)** Bifurcation diagram showing the branches of primary traveling wave solutions ($\mathrm{TW}_{\lambda_c}$) and excitable pulses (EPs) in periodic domains $L = \lambda_c = 2\pi/k_W \simeq 4$ and $L = 1000$, respectively. The branches are shown in terms of the maximal value of F-actin, $N$; solid lines indicate the linear stability regions of the solutions along the branch with respect to multiple copies of the wavelength. The inset shows a zoom-in of the uniform solutions as indicated by the bottom shaded region. **(c)** Enlargement of the EP solutions about their origin near the T-point, $A = A_{\mathrm{TP}}$, (see top shaded region). **(d)** Stability of EPs with respect to the domain size, $L$. **(e)** EP profiles along the branch in (**c**), as indicated by respective symbols. **(f)** Schematic low-dimensional geometrical interpretation for EP profiles in **e**.

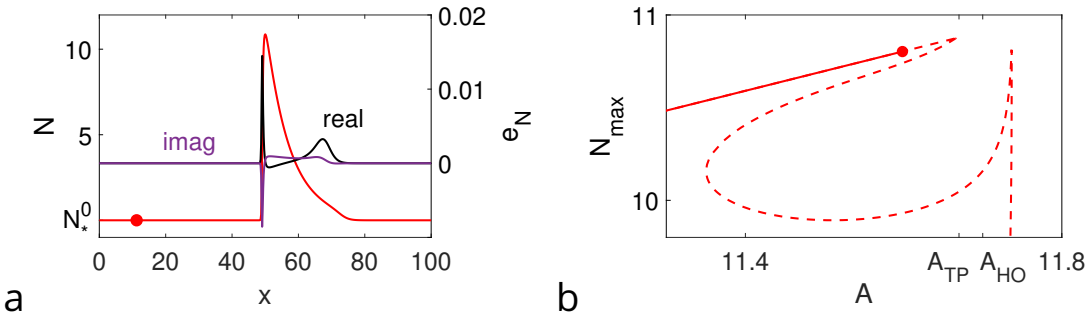


**Figure 4.** Instability mechanism of excitable pulses. **(a)** Selected unstable quasi-excitable pulse (EP) profile, computed in domain $L = 100$ (red line), and the respective normalized eigenfunction ($e_N$) computed at $A = 11.6$ near the T-point $A_{TP}$, as shown by the bullet in **(b)**. Parameters as in Methods and Materials Eq. 4.

Methods and Materials Fig. 5). Then the branch folds and continues as small amplitude unstable EPs. In practice, EP instability depends on the domain size (see Fig. 3**d**) and in the regime $O(\lambda_c) < L < O(10\lambda_c)$ it is triggered by the growth of a shoulder at the rear of the pulse solution (due to the proximity to the T-point, as $A \to A_{TP}$). We demonstrate this via the eigenfunction $e_N$ of the first growing unstable eigenvalue. The real part of $e_N$ exhibits a bumpy shape at the location of the pulse shoulder for $A \lesssim A_{TP}$ (see Fig. 4). In the context of the collisions discussed in ***Yochelis et al.*** (***2020***), the translational invariance is lost, and thus, since the perturbation in this range is of $O(1)$, the instability leads to the formation of standing waves that may resemble, but should not be confused with, the backfiring phenomenon ***Zimmermann et al.*** (***1997***); ***Nishiura and Ueyama*** (***2001***); ***Argentina et al.*** (***2004***); ***Manz and Steinbock*** (***2006***); ***Bauer et al.*** (***2015***).

## Discussion

Taken together, the rich and versatile spatiotemporal dynamics in the cell cortex is an essential part of actin-dependent cellular functions, such as phagocytosis, motility, macropinocytosis, and cell splitting. Nevertheless, the coexistence of different cortical patterns is poorly understood due to difficulties in systematically deciphering the underlying mechanisms. For example, based on visual and/or statistical inspections alone, it is too challenging to decide whether an observed spiral wave pattern results from an oscillatory, excitable, or bistable mechanism ***Allard and Mogilner*** (***2013***); ***Beta and Kruse*** (***2017***). In an attempt to address these fundamental questions of mechanisms, we used giant cells of the social amoeba *D. discoideum* as a model system, in which distinct coexisting actin wave patterns can be observed. Specifically, we observed that, in addition to the well-known wide, ring-shaped actin waves, a novel type of narrow, planar, and fast-moving solitary pulse emerged that exhibited the typical properties of an excitability medium, exhibiting, for example, mutual annihilation upon collision; see Fig. 1.

Motivated by these experimental observations, we performed a bifurcation analysis of a mass conserved activator-inhibitor model of actin signaling ***Bernitt et al.*** (***2017***); ***Yochelis et al.*** (***2020***), see Fig. 2, showing that even in a continuum-kinetic model that neglects most of the molecular details, essential features of pattern coexistence are revealed. Although we can envision other and more detailed models that may exhibit similar regimes of coexistence, the strength of our approach lies in uncovering the generic mechanism that leads to this behavior: a primary codimension-2 bifurcation and the evolution of homogeneous oscillations into excitable pulses via the so-called T-point (global) bifurcation in the presence of mass conservation. Specifically, using the total actin concentration as a control parameter, we revealed a regime, in which recurrent traveling wave patterns coexist with the more seldom emerging planar excitable pulses; see Fig. 3. The signature of this genuinely excitable regime is a low total actin concentration together with larger domain sizes, whereas in smaller domains and for higher actin concentrations, only traveling and/or standing waves are expected. This is in close qualitative agreement with the experimental observation that

excitable pulses only emerge in oversized giant cells.

More broadly, the mathematical setting of simultaneously arising homogeneous oscillations and waves, coupled to a large-scale mode, provides a novel extension not only of the existing approaches to intracellular patterns ***Shibata et al.*** (***2012***); ***Holmes and Edelstein-Keshet*** (***2012***); ***Allard and Mogilner*** (***2013***); ***Rappel and Edelstein-Keshet*** (***2017***); ***Bernitt et al.*** (***2017***); ***Beta and Kruse*** (***2017***); ***Beta et al.*** (***2020***); ***Liu et al.*** (***2021***) but also to biological pattern formation theory, in general. Nevertheless, due to the intrinsic role of mass conservation, this mechanism is particularly relevant for the enclosed context of a biological cell. Even though many more complex space-time patterns may coexist in cells, this specific case provides the first blueprint and a nontrivial additional step forward in the understanding of how the coexistence of functional patterns in cells, e.g., $Ca^{2+}$ waves ***Romeo and Jones*** (***2003***), can be comprehended and controlled based on the fundamental principles of pattern formation. In addition to a deeper understanding of the cortical pathologies that may lead, for example, to cancerous phenotypes and to uncontrolled tumor cell growth, we believe that our results will also inspire progress in the field of synthetic biology, in which minimal, yet robust, systems are required to reconstitute the essential features of a self-organized cell cortex.

## Methods and Materials

### Cell strains, culture conditions, and transformation

The axenic AX2 strain of *D. discoideum* was cultivated on a bacterial lawn of *Klebsiella aerogenes* on SM agar plates (peptone 10 g/l, yeast extract 1 g/l, glucose 10 g/l, $KH_2PO_4$ 1.9 g/l, $K_2HPO_4 \cdot 3H_2O$ 1.3 g/l, $MgSO_4$ anhydrous 0.49 g/l, 1.7% agar) or in 10-cm dishes with Sörensen's buffer (8 g $KH_2PO_4$, 1.16 g $Na_2HPO_4$, pH 6.0) supplemented with 50 $\mu$M $MgCl_2$, 50 $\mu$M $CaCl_2$ and containing *K. aerogenes* at an $OD_{600}$ of 2 at 22°C as described by Paschke *et al.* ***Paschke et al.*** (***2018***). The AX2 strain was adapted to growth in HL5 medium via macropinocytosis but it was still able to switch to growth based on phagocytosis of bacteria. To adapt them to these different growth conditions, the AX2 cells were cultivated for at least three days in a bacterial suspension or on SM agar plates with a bacterial lawn before they were used for the fusion protocol described below. A plasmid encoding for a Lifeact-GFP fusion protein was transformed into the AX2 cells by electroporation as previously described ***Flemming et al.*** (***2020***) with an ECM2001 electroporator (Harvard Apparatus, Holliston, MA, USA 01746-1388) using three square wave pulses of 500 V for 30 ms in electroporation cuvettes with a gap of 1 mm. Two plasmids for the expression of Lifeact-GFP were used: pDM138, which mediates G418 resistance ***Paschke et al.*** (***2018***), and pSF99, which mediates hygromycin resistance ***Flemming et al.*** (***2020***). Transformants were selected with either 33 µg/ml hygromycin (Invivogen, France) or $\mu$g/ml G418 (VWR, Germany) in 10-cm dishes and usually appeared 2-4 days post-transformation.

### Cell fusion

Fusion of AX2 *D. discoideum* cells grown on bacteria was performed according to the same protocol as the fusion of DdB *D. discoideum* cells described in ***Flemming et al.*** (***2020***). An amount of 1-$2 \times 10^8$ cells from an overnight shaking culture was washed and resuspended in Sörensen's buffer to a final concentration of $5 \times 10^7$ cells/ml to initiate development. The cells were then allowed to aggregate in buffer droplets with a volume of 1 ml for 2-3 h. Cell aggregates on top of the droplets were transferred to an electroporation cuvette (4 mm gap, VWR). Three square wave pulses of 1 kV for 70 $\mu$s were applied with 1 s intervals between each pulse using an ECM 2001 Electro Cell Manipulator (Harvard Apparatus, Holliston, MA, USA 01746-1388). Afterwards, the cells were immediately transferred to a tube containing 3 ml of Sörensen's buffer with an additional 2 mM $CaCl_2$ and 2 mM $MgCl_2$. After 1 min, 20-50 $\mu$l of cell suspension from the bottom of the tube was transferred for imaging to a 35-mm glass-bottomed microscopy dish (FluoroDish, World Precision Instruments). Wave formation was most abundant 3-6 h after the initiation of development.

## Live cell imaging

An LSM 780 (Zeiss, Jena) was used for live cell imaging. Excitation was performed with a 488-nm laser (GFP) and a 561-nm laser (RFP). Either a 63× (alpha Plan-Apochromat, NA 1.46, Oil Korr M27, Zeiss, Germany) or a 40× (Plan-Apochromat, NA 1.4 Oil DIC M27, Zeiss, Germany) objective lens was used. Images of the actin cortex were taken in a z-plane close to the surface-attached bottom membrane of the cell, where actin wave dynamics can be observed.

## Amplitude equations for the uniform oscillations and wave instability with mass conservation

The dispersion relation in Fig. 2**c** indicates a codimension-2 bifurcation that is associated with homogeneous oscillations (HO with onset at $k = 0$) and waves (onset at $k = k_W$). Standard symmetry considerations lead to amplitude equations from which $B_0$, $B_L$, $B_R$, and $C$ are obtained; see the center manifold reduction associated with (1) in the main text. The system of amplitude equations describes a weakly nonlinear approximation of the original model near the onsets and is generic (model independent),

$$\partial_t B_0 = \overbrace{r_0 B_0 - \beta \left|B_0\right|^2 B_0 + \delta_0 \partial_x^2 B_0}^{\text{CGLE for HO}} \overbrace{- \gamma_L \left|B_L\right|^2 B_0 - \gamma_R \left|B_R\right|^2 B_0 - \gamma_C C B_0}^{\text{coupling}} \overbrace{- \mu B_L B_R \overline{B}_0}^{\text{resonance}}, \tag{2a}$$

$$\left(\partial_t + s\partial_x\right) B_L = \overbrace{r_w B_L - b\left|B_L\right|^2 B_L - g_w \left|B_R\right|^2 B_L + \delta_w \partial_x^2 B_L}^{\text{CGLE for left TW}} \overbrace{- g_0 \left|B_0\right|^2 B_L - g_C C B_L}^{\text{coupling}} \overbrace{- m B_0^2 \overline{B}_R}^{\text{resonance}}, \tag{2b}$$

$$\left(\partial_t - s\partial_x\right) B_R = \overbrace{r_w B_R - b\left|B_R\right|^2 B_R - g_w \left|B_L\right|^2 B_R + \delta_w \partial_x^2 B_R}^{\text{CGLE for right TW}} \overbrace{- g_0 \left|B_0\right|^2 B_R - g_C C B_R}^{\text{coupling}} \overbrace{- m B_0^2 \overline{B}_L}^{\text{resonance}}, \tag{2c}$$

$$\partial_t C = \overbrace{\partial_x^2 \left[\delta_C C + \sigma_0 \left|B_0\right|^2 + \sigma_w \left(\left|B_L\right|^2 + \left|B_R\right|^2\right)\right]}^{\text{LSM}}, \tag{2d}$$

where $r_0$ and $r_w$ are related to the distance from the HO and wave instability onsets, with the critical wavenumbers and frequencies as $(k, \omega) = (0, \omega_0)$ and $(k, \omega) = (k_W, \omega_k)$, respectively, $\delta_C, \sigma_0, \sigma_w$ are the real parameters, and all the others are complex. Each of the oscillatory amplitudes ($B_0$, $B_{L/R}$) in (2) comprises the typical form of a complex Ginzburg-Landau equation (CGLE), a coupling term, and a term that may appear due to temporal resonances of $\omega_0$ and $\omega_k$. The parameters in (2) depend on the parameters of the original system and will be discussed elsewhere.

## Model equations and parameters

For the actin dynamics, we consider a three-component model (also see the text for details): $N(x,t)$ for F-actin, $S(x,t)$ for G-actin, and $I(x,t)$ for an inhibitor of actin polymerization. Following ***Yochelis et al.*** (***2020***), the model equations in dimensionless forms read:

$$\frac{\partial N}{\partial t} = \frac{N^2 S}{1+I} - N + D_{\mathrm{N}} \frac{\partial^2 N}{\partial x^2}, \tag{3a}$$

$$\frac{\partial S}{\partial t} = -\frac{N^2 S}{1+I} + N + D_{\mathrm{S}} \frac{\partial^2 S}{\partial x^2}, \tag{3b}$$

$$\frac{\partial I}{\partial t} = r_{\mathrm{N}} N - r_{\mathrm{I}} I + D_{\mathrm{I}} \frac{\partial^2 I}{\partial x^2}. \tag{3c}$$

To maintain fidelity with the experiments, we assume that $D_{\mathrm{I}} \ll D_{\mathrm{N}} < D_{\mathrm{S}}$ and $r_{\mathrm{I}} < r_{\mathrm{N}}$. For the analysis, we use the total number of actin monomers $A$ as a control parameter while keeping the rest of the parameters fixed (unless stated otherwise):

$$\left(D_{\mathrm{N}}, D_{\mathrm{S}}, D_{\mathrm{I}}, r_{\mathrm{N}}, r_{\mathrm{I}}\right) = (0.1, 1, 0.001, 2, 0.3)\,. \tag{4}$$

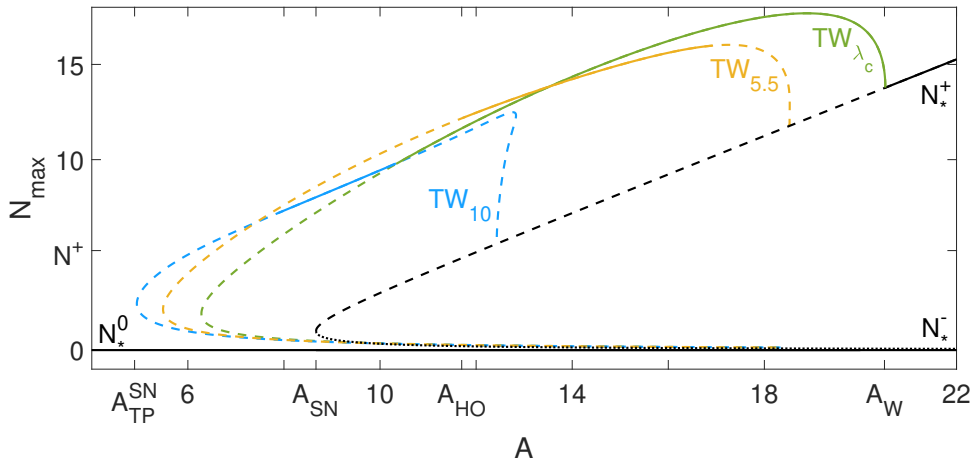


**Figure 5.** Bifurcation diagram (as in Fig. 3**b**) showing two additional branches of traveling wave (TW) solutions with wavelengths $\lambda = 5.5$ (orange) and $\lambda = 10$ (cyan); solid lines indicate linear stability with respect to multiple copies of the wavelength, and the subscripts correspond to the wavelength. Parameters as in (4).

## Linear stability of uniform and nonuniform solutions

System 3 has three uniform solutions ***Yochelis et al.*** (***2020***); one is referred to as trivial due to the absence of the activator

$$\mathbf{P}^0_* = (N^0_*, S^0_*, I^0_*) = (0, A, 0), \tag{5a}$$

while the other two are finite

$$\mathbf{P}^\pm_* = (N^\pm_*, S^\pm_*, I^\pm_*) = (N^\pm_*, A - N^\pm_*, aN^\pm_*), \tag{5b}$$

where $N^\pm_* = [A - a \pm \sqrt{(A-a)^2 - 4}]/2$ and $a = r_\mathrm{N}/r_\mathrm{I}$. While $\mathbf{P}^0_*$ always exists and, within the range of parameters considered here, is also stable, solutions $\mathbf{P}^\pm_*$ coexist for $A > A_\mathrm{SN} = a + 2$, where $\mathbf{P}^-_*$ is always unstable, and $\mathbf{P}^+_*$ is stable for $A > A_\mathrm{W}$. The linear stability onset of $\mathbf{P}^\pm_*$ is obtained following standard analysis to the linear order:

$$\mathbf{P}(x,t) - \mathbf{P}^\pm_* \propto e^{\sigma t + ikx}, \tag{6}$$

where $\sigma$ is a growth rate of the respective wave-number $k$. By inserting (6) into (3) and expanding to the linear order, we obtain the dispersion relations in Figs. 2**c** and 3**a**.

The existence of nonuniform solutions, such as TW and EP, was obtained using the numerical continuation package AUTO ***Doedel et al.*** (***2012***), after rewriting the system (3) in a comoving coordinate frame $x \to x + st$, where $s$ is the average translation speed at which these solutions propagate. The propagation speed is symmetric for left ($s > 0$) and right ($s < 0$) propagating solutions; hence, we employed periodic boundary conditions and only referred to one of these families. In this setting, TW and EP are steady state solutions, and to compute their stability, we retained the time derivatives employing a standard eigenvalue approach, with spatial derivatives being evaluated in the finite differences form. Linear stability is, however, determined for a large number of wavelengths (see also the main text), namely for $L = n\lambda$, where $\lambda$ is the TW wavelength, and $n$ is an integer, cf. ***Yochelis et al.*** (***2008***). In Figure 5, we show two representative TW solutions, $\lambda = 5.5$ (orange branch) and $\lambda = 10$ (cyan branch), together with the critical one denoted as $\mathrm{TW}_{\lambda_c}$ (green branch). We note that $\lambda \to \infty$ as $A \to A_\mathrm{HO}$.

## Acknowledgments

We thank Kirsten Sachse for technical assistance and Alexander Shevchenko for helpful discussions. C.B. acknowledges financial support by the Deutsche Forschungsgemeinschaft (DFG)- Project-ID 318763901 - SFB1294.

## References


**Allard J**, Mogilner A. Traveling waves in actin dynamics and cell motility. Curr Opin Cell Biol. 2013; 25(1):107–115.

**Argentina M**, Rudzick O, Velarde MG. On the back-firing instability. Chaos. 2004; 14(3):777–783.

**Asano Y**, Nagasaki A, Uyeda TQP. Correlated waves of actin filaments and PIP3 in Dictyostelium cells. Cell Motility and the Cytoskeleton. 2008; 65(12):923–934.

**Bauer PR**, Bonnefont A, Krischer K. Dissipative solitons and backfiring in the electrooxidation of CO on Pt. Scientific Reports. 2015; 5:16312.

**Bement WM**, Leda M, Moe AM, Kita AM, Larson ME, Golding AE, Pfeuti C, Su KC, Miller AL, Goryachev AB, et al. Activator–inhibitor coupling between Rho signalling and actin assembly makes the cell cortex an excitable medium. Nature Cell Biology. 2015; 17(11):1471–1483.

**Bernitt E**, Döbereiner HG, Gov NS, Yochelis A. Fronts and waves of actin polymerization in a bistability-based mechanism of circular dorsal ruffles. Nature Communications. 2017; 8:15863.

**Beta C**, Gov NS, Yochelis A. Why a large-scale mode can be essential for understanding intracellular actin waves. Cells. 2020; 9(6):1533.

**Beta C**, Kruse K. Intracellular oscillations and waves. Annual Review of Condensed Matter Physics. 2017; 8:239–264.

**Blanchoin L**, Boujemaa-Paterski R, Sykes C, Plastino J. Actin Dynamics, Architecture, and Mechanics in Cell Motility. Physiol Rev. 2014; 94(1):235–263.

**Cao Y**, Ghabache E, Rappel WJ. Plasticity of cell migration resulting from mechanochemical coupling. eLife. 2019; 8:e48478.

**Diz-Muñoz A**, Thurley K, Chintamen S, Altschuler SJ, Wu LF, Fletcher DA, Weiner OD. Membrane tension acts through PLD2 and mTORC2 to limit actin network assembly during neutrophil migration. PLoS Biology. 2016; 14(6):e1002474.

**Doedel EJ**, Champneys AR, Fairgrieve T, Kuznetsov Y, Oldeman B, Paffenroth R, Sandstede B, Wang X, Zhang C. AUTO07p: Continuation and bifurcation software for ordinary differential equations, Concordia University. . 2012; http://indy.cs.concordia.ca/auto.

**Doherty GJ**, McMahon HT. Mechanisms of Endocytosis. Ann Rev Biochem. 2009; 78(1):857–902.

**Falcke M**, Engel H, Neufeld M. Cluster formation, standing waves, and stripe patterns in oscillatory active media with local and global coupling. Physical Review E. 1995; 52(1):763.

**Fededa JP**, Gerlich DW. Molecular control of animal cell cytokinesis. Nature Cell Biology. 2012; 14(5):440–447.

**Flemming S**, Font F, Alonso S, Beta C. How cortical waves drive fission of motile cells. Proceedings of the National Academy of Sciences. 2020; 117(12):6330–6338.

**Gerhardt M**, Ecke M, Walz M, Stengl A, Beta C, Gerisch G. Actin and PIP3 waves in giant cells reveal the inherent length scale of an excited state. J Cell Sci. 2014 Oct; 127(20):4507–4517.

**Gerisch G**, Ecke M, Schroth-Diez B, Gerwig S, Engel U, Maddera L, Clarke M. Self-organizing actin waves as planar phagocytic cup structures. Cell Adhesion & Migration. 2009 Oct; 3(4):373–382.

**Gerisch G**, Bretschneider T, Müller-Taubenberger A, Simmeth E, Ecke M, Diez S, Anderson K. Mobile Actin Clusters and Traveling Waves in Cells Recovering from Actin Depolymerization. Biophys J. 2004; 87(5):3493–3503.

**Gerisch G**, Ecke M, Wischnewski D, Schroth-Diez B. Different modes of state transitions determine pattern in the Phosphatidylinositide-Actin system. BMC Cell Biology. 2011; 12(1):1–16.

**Gerisch G**, Ecke M, Neujahr R, Prassler J, Stengl A, Hoffmann M, Schwarz US, Neumann E. Membrane and actin reorganization in electropulse-induced cell fusion. J Cell Sci. 2013; 126(9):2069–2078.

**Glendinning P**, Sparrow C. T-points: a codimension two heteroclinic bifurcation. Journal of Statistical Physics. 1986; 43(3):479–488.

**Goehring NW**, Grill SW. Cell polarity: mechanochemical patterning. Trends in Cell Biology. 2013; 23(2):72–80.

**Holmes WR**, Edelstein-Keshet L. A comparison of computational models for eukaryotic cell shape and motility. PLoS Computational Biology. 2012; 8(12):e1002793.

**Hoon JL**, Wong WK, Koh CG. Functions and Regulation of Circular Dorsal Ruffles. Mol Cell Biol. 2012; 32(21):4246–57.

**Isaac EB**, Manor U, Kachar B, Yochelis A, Gov NS. Linking actin networks and cell membrane via a reaction-diffusion-elastic description of nonlinear filopodia initiation. Physical Review E. 2013; 88(2):022718.

**Ishikawa-Ankerhold HC**, Gerisch G, Müller-Taubenberger A. Genetic evidence for concerted control of actin dynamics in cytokinesis, endocytic traffic, and cell motility by coronin and Aip1. Cytoskeleton. 2010; 67(7):442–455.

**Janiaud B**, Pumir A, Bensimon D, Croquette V, Richter H, Kramer L. The Eckhaus instability for traveling waves. Physica D. 1992; 55(3-4):269–286.

**Jasnin M**, Beck F, Ecke M, Fukuda Y, Martinez-Sanchez A, Baumeister W, Gerisch G. The Architecture of Traveling Actin Waves Revealed by Cryo-Electron Tomography. Structure. 2019; 27(8):1211–1223.e5.

**Liu Y**, Rens EG, Edelstein-Keshet L. Spots, stripes, and spiral waves in models for static and motile cells. Journal of Mathematical Biology. 2021; 82(4):1–38.

**Lomakin AJ**, Lee KC, Han SJ, Bui DA, Davidson M, Mogilner A, Danuser G. Competition for actin between two distinct F-actin networks defines a bistable switch for cell polarization. Nature Cell Biology. 2015; 17(11):1435–1445.

**Luo W**, Yu Ch, Lieu ZZ, Allard J, Mogilner A, Sheetz MP, Bershadsky AD. Analysis of the local organization and dynamics of cellular actin networks. Journal of Cell Biology. 2013; 202(7):1057–1073.

**Manz N**, Steinbock O. Propagation failures, breathing pulses, and backfiring in an excitable reaction-diffusion system. Chaos. 2006; 16(3):037112.

**Masters TA**, Sheetz MP, Gauthier NC. F-actin waves, actin cortex disassembly and focal exocytosis driven by actin-phosphoinositide positive feedback. Cytoskeleton. 2016; 73(4):180–196.

**Miao Y**, Bhattacharya S, Banerjee T, Abubaker-Sharif B, Long Y, Inoue T, Iglesias PA, Devreotes PN. Wave patterns organize cellular protrusions and control cortical dynamics. Molecular Systems Biology. 2019; 15(3):e8585.

**Michaud A**, Swider ZT, Landino J, Leda M, Miller AL, von Dassow G, Goryachev AB, Bement WM. Cortical excitability and cell division. Current Biology. 2021; 31(10):R553–R559.

**Negrete Jr J**, Pumir A, Hsu HF, Westendorf C, Tarantola M, Beta C, Bodenschatz E. Noisy oscillations in the actin cytoskeleton of chemotactic amoeba. Physical Review Letters. 2016; 117(14):148102.

**Nishiura Y**, Ueyama D. Spatio-temporal chaos for the Gray–Scott model. Physica D. 2001; 150(3-4):137–162.

**Orth JD**, McNiven MA. Get Off My Back! Rapid Receptor Internalization through Circular Dorsal Ruffles. Cancer Res. 2006; 66(23):11094–96.

**Paschke P**, Knecht DA, Silale A, Traynor D, Williams TD, Thomason PA, Insall RH, Chubb JR, Kay RR, Veltman DM. Rapid and efficient genetic engineering of both wild type and axenic strains of Dictyostelium discoideum. PloS One. 2018; 13(5):e0196809.

**Rappel WJ**, Edelstein-Keshet L. Mechanisms of cell polarization. Curr Opin Syst Biol. 2017; 3:43–53.

**Romeo MM**, Jones CK. The stability of traveling calcium pulses in a pancreatic acinar cell. Physica D. 2003; 177(1-4):242–258.

**Sasaki AT**, Janetopoulos C, Lee S, Charest PG, Takeda K, Sundheimer LW, Meili R, Devreotes PN, Firtel RA. G protein–independent Ras/PI3K/F-actin circuit regulates basic cell motility. The Journal of Cell Biology. 2007; 178(2):185–191.

**Shibata T**, Nishikawa M, Matsuoka S, Ueda M. Modeling the self-organized phosphatidylinositol lipid signaling system in chemotactic cells using quantitative image analysis. Journal of Cell Science. 2012; 125(21):5138–5150.

**Stankevicins L**, Ecker N, Terriac E, Maiuri P, Schoppmeyer R, Vargas P, Lennon-Duménil AM, Piel M, Qu B, Hoth M, Kruse K, Lautenschläger F. Deterministic actin waves as generators of cell polarization cues. PNAS. 2020; 117(2):826–835.

**Tamemoto N**, Noguchi H. Reaction-Diffusion Waves Coupled with Membrane Curvature. Soft Matter. 2021; 17:6589.

**Tee YH**, Shemesh T, Thiagarajan V, Hariadi RF, Anderson KL, Page C, Volkmann N, Hanein D, Sivaramakrishnan S, Kozlov MM, et al. Cellular chirality arising from the self-organization of the actin cytoskeleton. Nature Cell Biology. 2015; 17(4):445–457.

**Turing A**. The chemical basis of morphogenesis. Phil Trans Roy Soc B. 1952; 237:37–72.

**Veltman DM**, Williams TD, Bloomfield G, Chen BC, Betzig E, Insall RH, Kay RR. A plasma membrane template for macropinocytic cups. eLife. 2016; 5:e20085.

**Vicker MG**, Xiang W, Plath PJ, Wosniok W. Pseudopodium extension and amoeboid locomotion in Dictyostelium discoideum: possible autowave behaviour of F-actin. Physica D. 1997; 101(3-4):317–332.

**Winterbottom D**, Matthews P, Cox SM. Oscillatory pattern formation with a conserved quantity. Nonlinearity. 2005; 18(3):1031.

**Yochelis A**, Knobloch E, Xie Y, Qu Z, Garfinkel A. Generation of finite wave trains in excitable media. Europhysics Letters. 2008; 83(6):64005.

**Yochelis A**, Beta C, Gov NS. Excitable solitons: Annihilation, crossover, and nucleation of pulses in mass-conserving activator-inhibitor media. Physical Review E. 2020; 101(2):022213.

**Zimmermann MG**, Firle SO, Natiello MA, Hildebrand M, Eiswirth M, Bär M, Bangia AK, Kevrekidis IG. Pulse bifurcation and transition to spatiotemporal chaos in an excitable reaction-diffusion model. Physica D. 1997; 110(1-2):92–104.